Journal of Molecular Catalysis A: Chemical 332 (2010) 45–52

Contents lists available at ScienceDirect

Journal of Molecular Catalysis A: Chemical

journal homepage: www.elsevier.com/locate/molcata

Hydrocarbon selective catalytic reduction of NO over Cu/Fe-pillared clays: Diffuse reflectance infrared spectroscopy studies

Fernando Dorado*, Prado Belén García, Antonio de Lucas, María Jesús Ramos, Amaya Romero

Department of Chemical Engineering, Faculty of Chemistry, University of Castilla-La Mancha, Av. Camilo José Cela, 10. 13005 Ciudad Real, Spain

ARTICLE INFO

Article history:
Received 4 June 2010
Received in revised form 27 July 2010
Accepted 17 August 2010
Available online 9 September 2010

Keywords:
Cu–Fe-PILC
DRIFTS
NO
Propene
SCR

ABSTRACT

The selective catalytic reduction (SCR) of NO was investigated by in situ diffuse reflectance infrared spectroscopy (DRIFTS) over catalysts based on iron-pillared clays (Fe-PILC) ion exchanged with copper. It was studied the influence of either total amount of metal or copper distribution as Cu^{2+} and CuO on the surface, with the aim to give a general idea of the reaction mechanism for this kind of catalysts. It was noted that the reaction intermediates were nitrates, nitrites, acetate, and $C_xH_yO_zN$ species. At low temperatures, bands corresponding to the vibration of C=C and COO^- groups were observed for those samples with CuO in their structure, confirming that its presence improves the NO yield to N_2.

1. Introduction

During the last few years, several works have been focussed on the development of the reaction mechanism for hydrocarbons selective catalytic reduction (HC-SCR) of NO. Some of them claimed that the reaction mechanism depended on both the adsorbates reactivity and their dynamic behaviour. On the other hand, the transition metals as well as the supports have given cause for controversy. Thus, Cant and Liu [1] summarized four potential mechanisms identified for Cu-MFI catalysts. It was suggested that the initial step of the HC-SCR process was the NO dissociation, whereas the hydrocarbon would remove the adsorbed oxygen which inhibited NO decomposition. A second proposal was the partial oxidation of hydrocarbons to produce species which achieved NO reduction. The third mechanism postulated that organonitrogen compounds were formed. Finally, the fourth one was that NO was first oxidized to the more effective oxidant (NO_2), followed by N_2 production through several degradations, starting from species containing carbon, nitrogen and oxygen. Other authors also proposed nitroparaffins or nitroso species as reaction intermediates over Cu-MFI [2,3].

Two reaction mechanisms have been proposed over Cu-ZSM-5. The first one proposed direct decomposition of NO over Cu. The hydrocarbon would play the role of oxygen elimination [4,5]. However, this mechanism cannot clear up neither the activity of zeolite pattern without copper nor the influence of the hydrocarbon nature. The second mechanism suggested that NO would be oxidized to NO_2 or nitrates; hydrocarbon would generate intermediate species acting as reducing agents towards NO. Then the NO_2 molecules or nitrates species would oxidize the hydrocarbon to give organo-nitro compounds which reacted with NO_x species to give N_2, CO_2 and water [6]. Other researches revealed by in situ FTIR spectroscopy over Cu–ZSM-5 the presence as intermediates of nitrites, nitrates, Cu^+–CO, –CN, –NCO, and –NH [7,8].

Other authors have studied the reaction mechanism of SCR of NO over catalysts based on oxides. Shimizu et al. [9] proposed a mechanism over Cu–Al_2O_3, where acetates and nitrates were found as reaction intermediates. Later, these intermediates reacted giving Cu–NCO which again reacted with nitrates or NO leading to N_2 and CO_2 as final products. Chi and Chuang [10] found over the same kind of catalysts C_3H_7–NO_2, Cu^0–CN and Cu^+–NCO over Cu^+/Cu^0. Sirilumpen et al. [11] studied the mechanism of SCR of NO over copper ion-exchanged aluminium pillared clays (Cu–Al-PILC). The limiting step was thought to be the N–N coupling between surface nitrate and gaseous nitric oxide to form nitrogen. Valverde et al. [12] proposed a reaction mechanism of SCR of NO by propene over Cu ion-exchanged titanium pillared clays (Cu–Ti-PILC). In situ FTIR studies showed that reaction intermediates were mainly nitrates, organo-nitro compounds and acetates. Cu^{2+}-OH groups reacted with the nitro group thus forming nitrate. The decomposition of nitrate species generated N_2 and a small amount of N_2O. C_3H_6 adsorption on the catalyst active sites was higher and stronger than NO adsorption and allowed the formation of hydrocarbon intermediates which were responsible for the NO reduction.

* Corresponding author. Tel.: +34 926295300; fax: +34 926295318.
E-mail address: Fernando.Dorado@uclm.es (F. Dorado).

1381-1169/$ – see front matter © 2010 Elsevier B.V. All rights reserved.
doi:10.1016/j.molcata.2010.08.019

In a previous work [13], Cu–Fe-PILC catalysts containing either isolated Cu^{n+} ions or CuO aggregates were prepared by ion-exchange using different pH values for the copper solution with the aim of identifying the nature and distribution of the copper species that were present. In this work, these catalysts have been studied by in situ diffuse reflectance infrared spectroscopy (DRIFTS) during the HC-SCR of NO to give a general idea about the reaction scheme mechanism.

2. Experimental

2.1. Catalyst preparation

The starting clay was a purified-grade bentonite (Fisher Company) with a particle size of <2 μm and a cation-exchange capacity of 97 mequiv g^{-1} dry clay. A $FeCl_3{\cdot}6H_2O$ solution was added to NaOH solutions to obtain the required OH/Fe molar ratio. In order to avoid precipitation of iron species, the pH was kept constant at 1.7. The mixture was aged for 4 h under stirring at room temperature. The pillaring solution was then added dropwise to an aqueous clay suspension. The mixture was kept under vigorous stirring for 12 h at room temperature. Finally, the solid was washed, dried, and calcined for 2 h at 400 °C.

Metal was introduced by conventional ion-exchange using 100 mL of metal aqueous solution per gram of iron-pillared clay. A range of copper-exchanged Fe-PILC samples were prepared with solutions of $Cu(CH_3COO)_2{\cdot}H_2O$, and the pH then adjusted by the addition of aqueous ammonia to give the desired final pH. All catalysts were calcined for 2 h at 400 °C. These catalysts are referred to as a function of the metal content and the pH of the ion-exchange solution. For instance, Cu3.3–5.4 corresponds to a catalyst ion exchanged with copper, leading to a loading of this metal of 3.3 wt.% using a solution with a pH equal to 5.4. More details about catalysts preparation can be found elsewhere [13–15].

2.2. DRIFT experiments

In situ IR spectra were collected with a Perkin-Elmer FTIR Spectrum GX spectrometer, by accumulating 100 scans at a resolution of 4 cm^{-1}. The focused wavenumber range was 4000–1000 cm^{-1}. The sample was placed in the middle of a high-temperature reaction DRIFT chamber with KBr windows (Harrick). The temperature was measured with a K-type thermocouple and controlled with an automatic temperature controller (Harrick).

Prior to each experiment, 0.05 g of catalyst was heated at a rate of 10 °C/min from room temperature to 400 °C. After a period of 30 min at this temperature, the sample was later cooled to 200 °C at 10 °C/min in a He flow of 60 mL min^{-1}. After pretreatment, the background spectrum of a He flow of 25 mL min^{-1} was collected at 200 °C. Then, the flow of a gas mixture was switched to the DRIFT chamber with a GHSV of 15,000 h^{-1}. The reaction gases for adsorption studies were: NO/He (0.1/99.9), NO/O_2/He (0.1/5/94.9), C_3H_6/He (0.1/99.9), C_3H_6/O_2/He (0.1/5/94.9). For reactivity tests, the reaction mixture was $NO/O_2/C_3H_6$/He (0.1/5/0.1/94.8).

2.3. Catalyst characterization

To quantify the total amount of the metals incorporated into the catalyst, atomic absorption spectroscopy measurements were made, using a SPECTRAA model 220FS analyzer, with an error of ±1%. The samples were previously dissolved in hydrofluoric acid and diluted to the interval of measurement.

Surface area and pore volumes were determined by nitrogen adsorption at 77 K in a static volumetric apparatus (Micromeritics ASAP 2010 sorptometer). Pillared clays were outgassed prior to use at 180 °C for 16 h under a vacuum of 6.6×10^{-9} bar. Specific total surface areas were calculated using the Brunauer–Emmett–Teller (BET) equation, whereas specific total pore volumes were evaluated from the nitrogen uptake at a N_2 relative pressure of $P/P_0 = 0.99$. The t-plot method was used to determine the micropore surface area and micropore volume.

The total acid-site density and acid-strength distribution were measured by temperature-programmed desorption of ammonia (TPDA), using a Micromeritics TPD/TPR 2900 analyzer with a thermal conductivity detector. The following procedure was described in detail in [13]. The average relative error in the acidity determination was <3%.

Temperature-programmed reduction (TPR) measurements were carried out with the same apparatus as described above following the procedure described in [13]. TPR profiles were reproducible, with standard deviations for the temperature of the peak maxima being <1%.

2.4. Catalytic tests

Activity experiments were carried out at atmospheric pressure in a flow-type apparatus designed for continuous operation at atmospheric pressure. This apparatus consisted of a gas feed system for each component, with individual control by mass flowmeters, a fixed-bed downflow reactor, and an exit gas flowmeter. The reactor, a stainless steel tube with an internal diameter of 4 mm, was filled with the catalyst sample (0.25 g). A temperature programmer was used with a K-type thermocouple that was installed in contact with the catalyst bed. The products were analyzed simultaneously, using a chemiluminiscence analyzer ($NO–NO_2–NO_x$ ECO PHYSICS) and a Fourier transform infrared (FTIR) analyzer (Perkin-Elmer Spectrum GX) that was capable of measuring the following species continuously and simultaneously: NO, NO_2, N_2O, CO_2 and C_3H_6.

The feed composition was as follow: 1000 ppm C_3H_6, 1000 ppm NO, 5% O_2 and the balance He. The feed gases were mixed and preheated before entering the reactor. The space velocity (GHSV) was 15,000 h^{-1}, and the flow rate was 125 mL/min. Before the reaction was started, the catalysts were preconditioned at 400 °C under a flow of helium (125 mL/min) for 60 min. Then, the temperature was down to 200 °C. The reaction measurements for each temperature were carried out after 2 h to ensure that the steady state was reached. All experiments were tested for reproducibility with analytical repeatability, with an error in NO conversion of <5%.

3. Results and discussion

3.1. Catalyst characterization and catalytic activity

Fig. 1 shows the X-ray diffraction (XRD) patterns for the parent Fe-PILC calcined at 400 °C and for the original clay. The XRD pattern for the parent clay exhibited a main peak at 2θ about 9° which it is commonly assigned to the basal (0 0 1) reflection (d_{001}). Peak corresponding to the (0 0 1) reflection for Fe-PILC appeared at smaller 2θ angles ($2\theta \approx 4°$). This fact clearly indicated an enlargement of the basal spacing of the clay as a consequence of the pillaring process. For this last sample a wider peak in the range $2\theta \approx 7–8°$ was observed, which can be attributed to two overlapped peaks: the (0 0 2) reflection of the pillared clay and to the (0 0 1) reflection corresponding to the intercalation of a proportion of monomeric species of small size, similar as those reported by Valverde et al. [16] for Ti-PILCs, thus leading to smaller openings of the clay layers [17].

The interlayer spacing for Na-montmorillonite, originally occupied by hydrated Na^+ cations, was about 3.5 Å. After calcination, the clay structure collapsed (d_{001} decreased to 9.7 Å) and the inter-

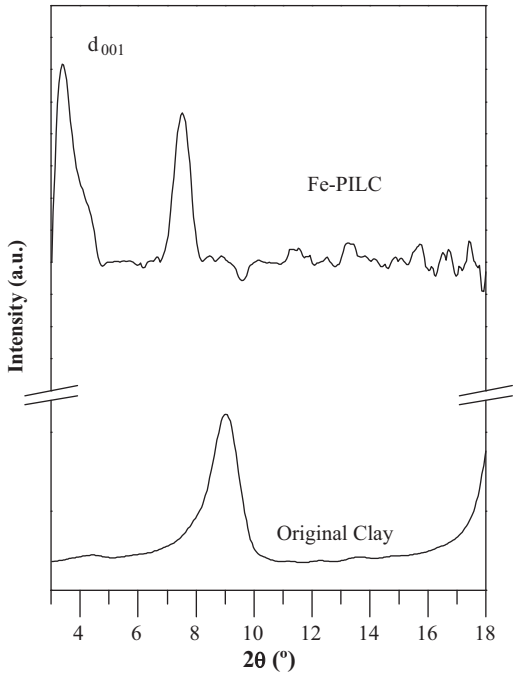

Fig. 1. X-ray diffraction (XRD) patterns for the parent Fe-PILC calcined at 400 °C and for the original clay.

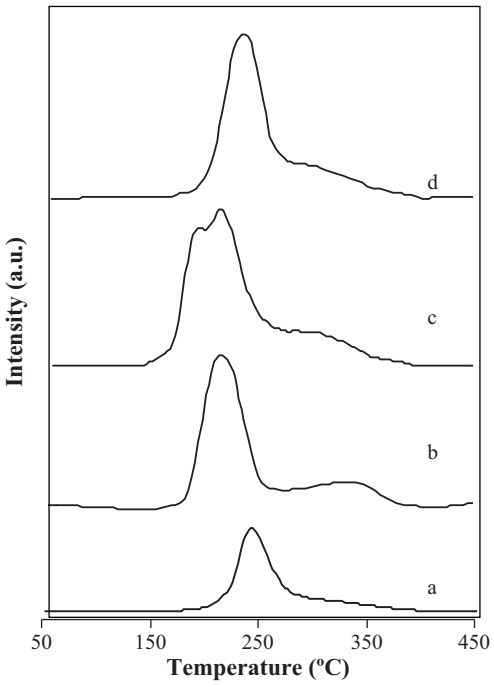

Fig. 2. H_2-TPR profiles for samples: (a) Cu3.7–5.6, (b) Cu4.8–7.0, (c) Cu6.2–9.0 and (d) Cu6.5–10.5.

layer region became inaccessible to the N_2 molecules. Large and hydrated Fe polyoxocations introduced into the interlayer spaces of the clay push the sheets apart by about 15 Å (25 Å corresponding to d_{001} minus 9.6 Å corresponding to the thickness of the layers). Calcination of the Fe-pillared clays led to the dehydration and dehydroxylation of Fe polycations and gave rise to the formation of polymeric Fe_2O_3 species, which permanently link adjacent layers.

The textural characteristics of the iron-pillared clay are summarized in Table 1. The surface area analysis would indicate that the pillaring process produced a significant increase in the surface area, from 36 m^2/g (for the original clay) to 285 m^2/g (for the parent Fe-PILC), due mainly to micropores formation. In this case, the micropore area represented the major part (86%) of the total surface area. On the other hand, it can be observed that the total acidity of the clay was enhanced approximately three times, due to the pillaring process (Table 1).

The results for the Cu catalysts characterization were discussed in detail in a previous work [13] and they will be summarized here. The composition and characteristics of Cu-exchanged iron-pillared clays are given in Table 1. The copper content of the catalysts was modified by two different ways: (a) without pH control (using an aqueous Cu solution concentration of 0.1 M (sample Cu3.3–5.4) and (b) controlling the pH of the ion-exchange step with copper from 7.0 to 10.5 (samples Cu4.8–7.0, Cu6.2–9.0 and Cu6.5–10.5). As observed, an increase of the Cu loading led to a decrease of the surface area (mainly the micropore area) and the micropore volume of the catalyst. This may be consequence of a partial blocking of the pillaring matrix by the metal species located in the interlayer areas [13].

Fig. 2 shows the TPR profiles for the samples. First of all, it should be noted that the aim of the TPR experiments is to analyze the Cu species. However, the parent Fe-PILC showed a small reduction peak at 350–370 °C due to the $Fe^{3+} \rightarrow Fe^{2+}$ reduction process [14]. To avoid interferences, this peak was always accounted for without significant error by subtraction in the TPR profiles. For the catalysts here prepared, it should be taken into account that the copper is not only present as Cu^{2+} ions chemically bonded to the pillars of the clay, but also as CuO clusters. The presence of these oxygenated clusters can be explained considering the Cu solution behaviour under basic pH, when it is added NH_3 to the acetate copper solution [13]. Thus, it can be observed the $Cu(OH)_2$ precipitation as well as the change of the colour of solution, which turns to the characteristic blue provided by the $[Cu(NH_3)_4]^{2+}$ complex ($Cu(OH)_2 + 4NH_3 \leftrightarrow [Cu(NH_3)_4]^{2+} + 2OH^-$). After calcination, these compounds form CuO and isolated Cu^{2+}, respectively. Under these test conditions, the sample Cu3.3–5.4 showed one reduction peak at around 250 °C, assigned to the reduction of Cu^{2+} to Cu^+. The catalyst Cu4.8–7.0 showed two reduction peaks. The first peak, centered at

Table 1
Composition and characteristics of the catalysts.

Sample	Cu (wt.%)	pH	Cu solution (M)	S_{BET} (m^2/g)[a]	S_{int} (m^2/g)[a]	V_p (cm^3/g)[b]	$V_{\mu p}$ (cm^3/g)[b]	Total acidity (mmol NH_3/g)	Max. NO conversion (%)[c]	Yield C_3H_6 to CO_2 (%)
Fe-PILC	–	–	–	285	247 (86)	0.187	0.126	0.317	–	–
Cu3.3–5.4	3.3	5.4	0.1	245	211 (86)	0.181	0.123	0.506	36.2 (280 °C)	81.5
Cu4.8–7.0	4.8	7.0	0.01	230	177 (77)	0.183	0.105	0.518	43.0 (260 °C)	81.2
Cu6.2–9.0	6.2	9.0	0.01	214	158 (74)	0.177	0.100	0.495	53.9 (260 °C)	86.7
Cu6.5–10.5	6.5	10.5	0.005	210	147 (70)	0.177	0.097	0.404	45.2 (280 °C)	95.6

[a] Total surface area obtained from the BET equation (S_{BET}). Micropore area obtained from the t-plot method (S_{int}). % of the total surface area in brackets.
[b] Micropore volume obtained from the t-plot method ($V_{\mu p}$) and total pore volume at $P/P_0 = 0.99$ (V_P).
[c] Reaction conditions: NO = C_3H_6 = 1000 ppm, O_2 = 5 wt.%, He = balance, catalyst = 0.25 g, and total flow rate = 125 mL/min.

210 °C, was attributed to the overlapping of the reduction reaction of Cu^{2+} to Cu^{+} and CuO to Cu^{0}. The second peak, less pronounced and about 350 °C, was assigned to the reduction of Cu^{+} to Cu^{0}. Sample Cu6.2–9.0 showed a broad peak at 210 °C, attributed to the reduction of Cu^{2+} to Cu^{+} with a shoulder at 180 °C, assigned to the reduction of CuO to Cu^{0}. Finally, the sample Cu6.5–10.5 presented one peak centered at 240 °C, which was also attributed to the overlapping of the reduction reactions of Cu^{2+} to Cu^{+} and CuO to Cu^{0}. Note that the reduction peak attributed to the reduction of both CuO and Cu^{2+} species was unresolved for the samples Cu4.8–7.0 and Cu6.5–10.5 (these peaks were overlapped). However, there is a better resolution for the sample Cu6.2–9.0 which suggests the presence of a higher proportion of Cu^{2+} ions under the influence of CuO clusters in this sample. Finally, for the sample Cu3.3–5.4 (prepared without pH control), copper was mainly present as isolated Cu^{2+}, not as CuO.

On the other hand, acidity of ion-exchanged pillared clays (Table 1) depended on both the ion-exchanged transition metal (Cu in this study) and the metal loading. It can be observed that the total acidity decreased when the Cu content was increased in samples prepared with pH control. As mentioned above, this fact is in concordance with the TPR profiles, showing higher acidity values those samples which have in their structure more Cu^{2+} ions. Moreover, taken into consideration that CuO clusters have a low participation in the total acidity (they adsorb NH_3 very weakly [13]), the acidity of sample Cu3.3–5.4, quite similar to that of sample Cu4.8–7.0 despite its lower metal content, seems logical.

In brief, the sample prepared without pH control (Cu3.3–5.4) showed in its structure only isolated Cu^{2+} ions, while samples prepared under alkali conditions showed in their structure copper both as Cu^{2+} and CuO clusters, increasing the proportion CuO/Cu^{2+} with the pH value. Note that the sample Cu6.5–10.5 shows the highest decrease of the surface area and pore volume (Table 1), which may be due to the higher proportion of copper species as CuO located at the outer surface of the catalyst. These clusters would be blocking the pores, explaining the textural characteristics of this sample.

The characterization results would be consistent with the catalytic activity tests (Table 1). Thus, sample Cu6.2–9.0 gave the best activity for C_3H_6 combustion to CO_2 at temperatures below 260 °C which was related to the presence of Cu^{2+} active sites under the influence of CuO clusters. This easier C_3H_6 oxidation favoured the NO_x reduction at low temperature. On the contrary, the sample Cu6.5–10.5, with similar Cu loading, showed a poorer activity at higher temperature, suggesting again that there was in its structure less catalytic copper specie (Cu^{2+}) under the influence of CuO clusters.

3.2. NO adsorption over Cu–Fe-PILC catalysts

Fig. 3(A) shows the IR spectra after NO adsorption at room temperature over the four catalysts studied. According to Hadjiivanov et al. [18], the most important bands found in Fig. 3(A) can be assigned to several vibration modes of nitro, nitrites and nitrates species. Thus, band at 1626 cm^{-1} can be attributed to bridging bidentate nitrates on Cu^{2+} ions [8,10,11,15]. Band at 1550 cm^{-1} was assigned to chelating bidentate nitrates anchored on Cu^{2+} species [8,10,15]. The assignment of bands at 1497, 1449, and 1417 cm^{-1} has not been well defined but it could be possible to assign them to the ν_3 vibration mode of monodentate nitrates [13]. Band at 1368 cm^{-1} was attributed to ν(N=O) vibration mode of bridging monodentate nitrites [15] or organic nitro compounds [13], while band at 1319 cm^{-1} was assigned to $\nu_s(NO_2)$ vibration mode of nitro species [11,15].

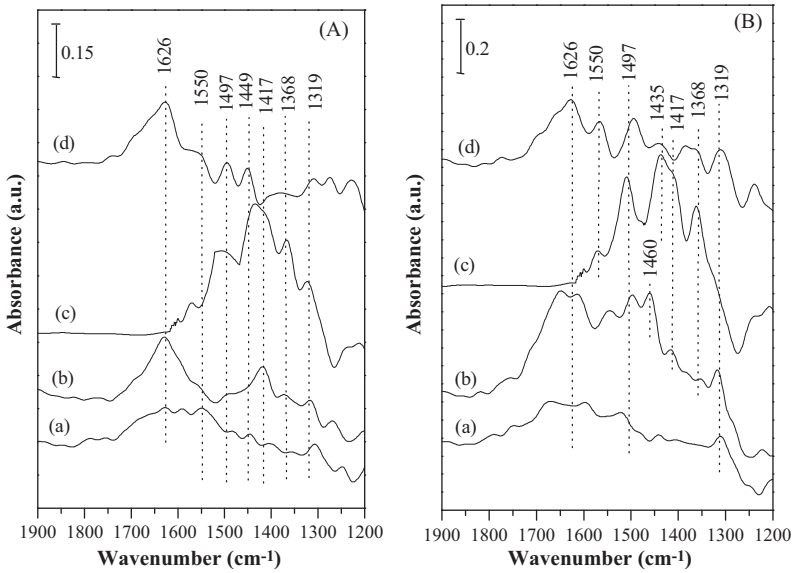

wavenumber (cm^{-1})	Band assignation	References
1626	Bridging bidentate nitrates	8, 10, 11, 15
1550	Chelating bidentate nitrates	
1497 1449 1417	monodentate nitrates	13
1368	monodentate nitrites ν(N=O) organic nitro compounds	15, 13
1319	nitro species, $\nu_s(NO_2)$	11, 15

Fig. 3. (A) NO/He adsorption, (B) NO/O_2/He adsorption at room temperature over (a) Cu3.3–5.4, (b) Cu4.8–7.0, (c) Cu6.2–9.0 and (d) Cu6.5–10.5.

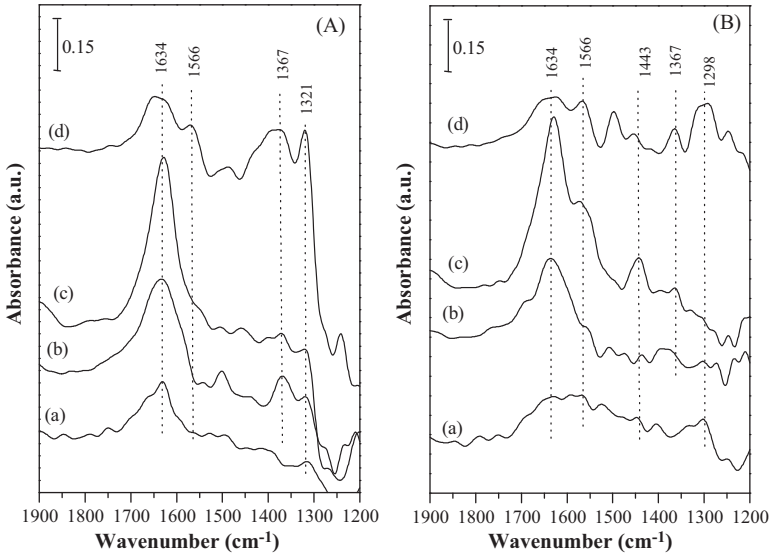

wavenumber (cm^{-1})	Band assignation	References
1634	C=C stretching vibration	6, 10, 16, 17
1566	C – H bond vibration	16, 18
1443	(COO^-) stretching vibrations (acetate adsorbed)	9, 10, 12, 20
1367	CH_3 deformation vibration or	17, 18, 19, 21
1321	CHO deformation vibration	
1298	C-C stretching vibration	21

Fig. 4. (A) C_3H_6/He adsorption, (B) C_3H_6/O_2/He adsorption at room temperature over (a) Cu3.3–5.4, (b) Cu4.8–7.0, (c) Cu6.2–9.0 and (d) Cu6.5–10.5.

IR spectrum of catalyst Cu3.3–5.4 shows wide and undefined bands which could be likely ascribed to the adsorption of bridging bidentate nitrates anchored on Cu^{2+} species. For the sample Cu4.8–7.0, bands attributed to both kinds of bidentate nitrates and also those of monodentate nitrates were sharper. Catalyst Cu6.2–9.0 spectrum showed very sharp and well defined bands attributed principally to monodentate nitrates but also intense bands corresponding to nitro and monodentate nitrite species. Note that bands attributed to bridging bidentate nitrates were no present at all. Finally, Cu6.5–10.5 spectrum showed not very well defined bands in the entire spectrum of the vibration modes of nitro, nitrites and monodentate nitrates species (1600–1300 cm^{-1}) due to that, as it has already been commented, there was less amount of Cu^{2+} species influenced by CuO clusters. Nevertheless, note that band corresponding to bridging bidentate nitrate was more pronounced (similar to catalyst Cu4.8–7.0).

Summarizing, NO adsorption studies led to the following considerations: the adsorption of bridging bidentate nitrates species could be attributed to the presence in the catalyst structure of isolated Cu^{2+} ions (without or poor influence of CuO clusters), whereas

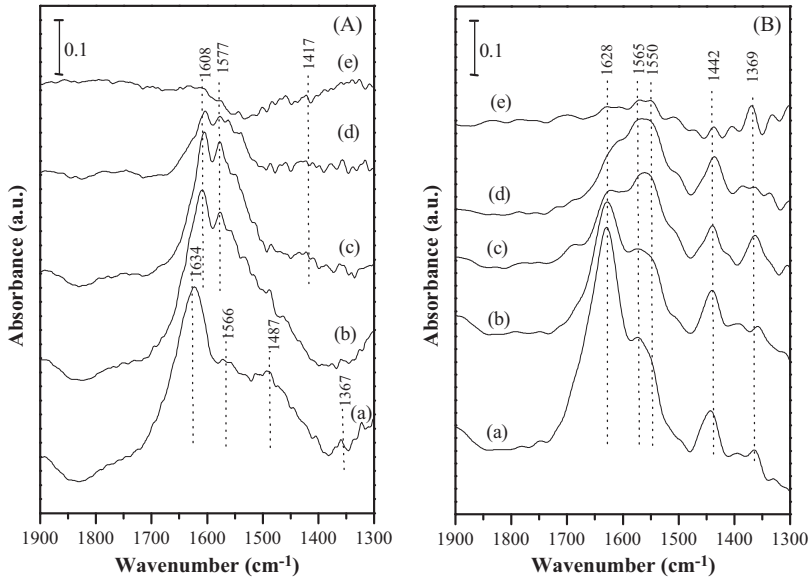

Fig. 5. (A) NO/O_2/He adsorption over Cu4.8–7.0 after saturation with C_3H_6, (B) C_3H_6/O_2/He adsorption over Cu4.8–7.0 after saturation with NO at (a) 30 °C, (b) 100 °C, (c) 200 °C, (d) 300 °C and (e) 400 °C.

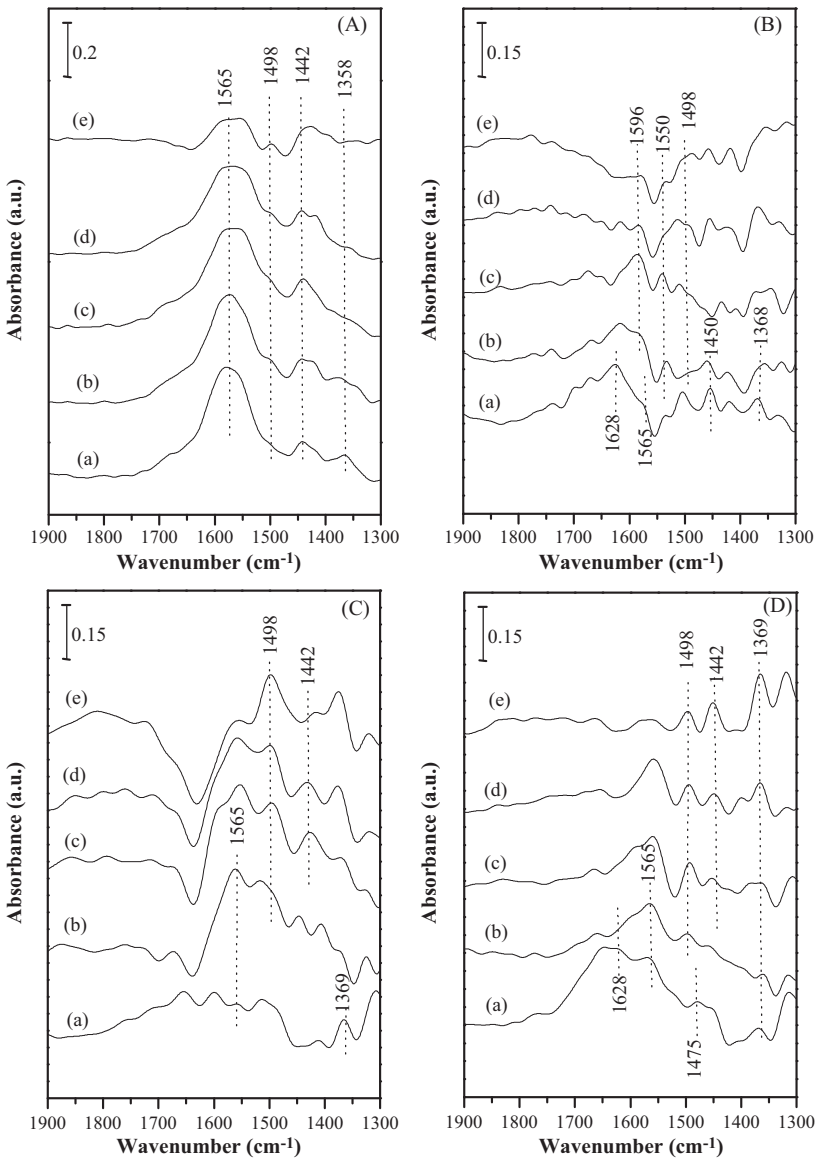

Fig. 6. In situ DRIFTS spectra of C_3H_6–SCR of NO over (A) Cu3.3–5.4, (B) Cu4.8–7.0, (C) Cu6.2–9.0 and (D) Cu6.5–10.5 catalysts at (a) 30 °C, (b) 100 °C, (c) 200 °C, (d) 300 °C and (e) 400 °C. Reaction conditions: NO = C_3H_6 = 1000 ppm, O_2 = 5 wt.%, He = balance, catalyst = 0.05 g, and GHSV of 15,000 h^{-1}.

the adsorption of nitro groups, monodentate nitrites and monodentate nitrates could be assigned to the presence in the catalyst of Cu^{2+} ions under the influence of neighbour CuO clusters.In the study of NO adsorption under the presence of oxygen (Fig. 3(B)), similar bands as in absence of oxygen were observed. However, the intensity of the bands was higher indicating that the adsorption of nitrates, nitrites and nitro group were highly favoured in the presence of oxygen [9].

3.3. C_3H_6 adsorption over Cu–Fe-PILC catalysts

Fig. 4(A) shows the IR spectra after propene adsorption at room temperature. Bands in the 1650–1300 cm^{-1} region, corresponding to vibration of hydrocarbon species can be observed. Band at 1634 cm^{-1} was assigned to stretching vibration mode ν(C=C) [6,10,19,20]. Band at 1566 cm^{-1} can be attributed to bending of C–H bond [19,21]. Bands at 1367 and 1321 cm^{-1} were assigned to different vibration modes of CH_3 [20–22].

In the presence of oxygen (Fig. 4(B)), additional new bands were observed. These bands can be due to the adsorption of oxidized hydrocarbon which could be formed after reaction between oxygen and propene. Bands at 1443 cm^{-1} were attributed to (COO^-) stretching vibrations of the adsorbed acetate [9,10,12,23]. Band at 1367 cm^{-1} was assigned to the CH_3 deformation vibrations [22,24] and also it could be assigned to CHO deformation vibration of a formate group [20]. Finally, band at 1298 cm^{-1} was attributed to C–C stretching vibration [24].

In general, the intensity of the bands corresponding to adsorption of hydrocarbon species (oxidized or not) was higher for those samples where the active sites (Cu^{2+}) were significantly influenced by neighbour CuO clusters (Cu4.8–7.0 and Cu6.2–9.0).

3.4. Temperature-programmed surface reaction (TPRS) studies

TPRS runs with the sample Cu4.8–7.0 were carried out with the aim of identifying reaction intermediates and studying the evolution of the adsorption bands associated to the active sites of the catalyst. For the chosen sample, copper species were both as isolated Cu^{2+} ions and CuO clusters. Before the first TPRS experiment, the sample was exposed to a C_3H_6/He (0.1/99.9) stream for 1 h at room temperature, followed by He purge at room temperature for 30 min. After that, the sample was put in contact with a mixture of

$NO/O_2/He$ (0.1/5/94.9) and the TPRS run started. Spectra recorded in the TPRS experiment from 30 to 400 °C are shown in Fig. 5(A). The second TPRS run was carried out after the exposure to the sample to a NO/He (0.1/99.9) flow for 1 h at room temperature, and further He purge. IR spectra recorded under flow of $C_3H_6/O_2/He$ (0.1/5/94.9) during the TPRS experiment from 30 to 400 °C with a heating rate of 10 °C/min are represented in Fig. 5(B).

In Fig. 5(A), for the spectrum (a) at room temperature, different bands attributed to anchored hydrocarbons were predominant (band at 1634 cm^{-1} assigned to stretching vibration mode ν(C=C) [6,10,19,20]; bands at 1487 and 1566 cm^{-1} corresponding to bending of C–H bond [19,21] and band at 1367 cm^{-1} assigned to the CH_3 deformation vibrations [22,24]). Nevertheless, when the temperature increased, these bands start to vanish and others corresponding to bridging bidentate nitrates vibration (1608 cm^{-1}), chelating bidentate nitrates (1577 cm^{-1}) and monodentate nitrates vibration (around 1417 cm^{-1}) became predominant. Moreover, the intensity of these bands increased with the temperature up to 300 °C, temperature at which begun to decrease, disappearing almost completely at 400 °C.

In Fig. 5(B), it can be observed that, at room temperature (for which hydrocarbon combustion is not favoured), bands attributed to bridging and chelating bidentate nitrates vibration (1628 and 1565 cm^{-1}), vibration of nitro groups of the organo-nitro compounds (R–NO_2) (can be attributed also to band at 1565 cm^{-1}) [10,12,20,25], and ν(N=O) vibration mode of monodentate nitrites [11,15] (1442 and 1362 cm^{-1}) were observed. However, at higher temperatures (100 °C) the propene combustion started to be favoured and the exposure to $C_3H_6/O_2/He$ could lead to some significant changes in the assignment of the bands. Thus, it could be appreciated an intensity increase of the bands related to the presence of oxidized hydrocarbons in the temperature range between 100 and 300 °C (band at 1442 cm^{-1} assigned to the vibration of the COO^- group, band at 1565 cm^{-1} attributed in this case, to the C–C stretching vibration [24] and band at 1369 cm^{-1} corresponding to the deformation vibrations of the group $\delta(CH_3)$ [22]). These results were in agreement with the copper species distribution found for the sample Cu4.8–7.0, where both isolated Cu^{2+} ions and CuO clusters were present, providing the later a promoting effect for the propene oxidation at low temperature [13].

3.5. DRIFT experiments at steady state conditions

Fig. 6 shows the adsorbed species over Cu–Fe-PILC catalysts under the exposure to the reaction mixtures as a function of the temperature. All samples presented common bands, which had previously observed in adsorption and TPRS experiments, but some of them could have different relative intensities [26].

According to the assignment of the bands in the recorded spectra at steady state conditions, the reaction intermediates found were, mainly, nitrates and organo-nitro and organo-nitrito compounds at low temperatures (30 °C), and oxidized hydrocarbons (mainly acetate) at higher temperatures.

Thus, the most important bands at low temperature were: bands at 1628 cm^{-1} corresponding to bridging bidentate nitrates, bands at 1565 cm^{-1} corresponding to the vibration of nitro groups of the possible organo-nitro compounds (R–NO_2) formed after interaction between the hydrocarbon and the mixture NO/O_2 over the catalyst surface [10,12,20,25], bands at 1450 cm^{-1} corresponding to monodentate nitrates and bands at 1369 cm^{-1} corresponding to monodentate nitrites [15]. On the other hand, at higher temperatures, the most important bands were: band at 1498 cm^{-1} corresponding to bending of C–H bond [19,21] and band at 1442 cm^{-1} corresponding to CH_3–COO^- compound (this compound could be also appear at 1550 cm^{-1}) [9,10,12,23].

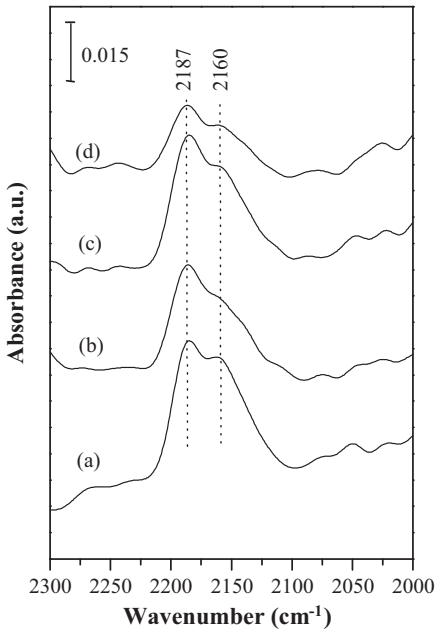

Fig. 7. DRIFTS spectra in the isocyanate region under reaction conditions at 300 °C over (a) Cu3.3–5.4, (b) Cu4.8–7.0, (c) Cu6.2–9.0 and (d) Cu6.5–10.5. NO = C_3H_6 = 1000 ppm, O_2 = 5 wt.%, He = balance, catalyst = 0.05 g, and GHSV of 15,000 h^{-1}.

On the other hand, several authors have postulated, for the same reaction over other kind of catalysts, the presence of isocyanates as a possible reaction intermediate. Thus, over CuO/Al_2O_3, Chi and Chuang [10] found a band at 2237 cm^{-1} attributed to Cu^+–NCO. Shimizu et al. [9] found bands at 2236 and 2198 cm^{-1} assigned to Al–NCO and Cu–NCO, respectively, where Al–NCO species could be a relatively inert spectator on the surface, whereas Cu–NCO species were postulated as real reaction intermediates. Reaction intermediates suggested for the C_3H_6–SCR over Cu–ZSM-5 [7] are R–NO_x and –CN, which is transformed to –NCO. Further transformation of –NCO would occur by its hydrolysis into –NH and NH_3. Then, ammonia molecules would react with NO to lead to N_2. Moreover, other authors have suggested –NCO as reaction intermediate of the SCR–NO by hydrocarbons over other catalysts modified with several transition metals. Thus, bands at 2194 and 2227 cm^{-1} attributed to isocyanates adsorbed on Ni were found in the study of Ni/NaMOR [20]. When Pd–Al_2O_3 was used as catalyst, bands at 2253 and 2232 cm^{-1} assigned to Al–NCO were also detected [27]. On Co–ZSM-5, a band at 2160 cm^{-1} was attributed to isocyanate [28], while NCO bands over Ni/AgMOR and Co/AgMOR appeared at 2166 cm^{-1} [29]. The spectrum in the appropriate range (2000–2300 cm^{-1}) was collected over the four Cu–Fe-PILC catalysts studied at steady state conditions (Fig. 7), in order to confirm the presence or absence of isocyanates species. Thus, bands at 2160 and 2187 cm^{-1} were assigned to isocyanate adsorbed over both isolated Cu^{2+} and Cu^{2+} ions under the influence of neighbour CuO clusters. Bands in the region between 3300 and 3100 cm^{-1}, related to the presence of ammonia, were not detected (not shown). It may be due to the fast hydrolysis of NCO species to ammonia under reaction conditions, since water is available as reaction product. Then, this step cannot be excluded from the reaction mechanism of C_3H_6–SCR over Cu–Fe-PILC.

Regarding the results obtained from DRIFTS experiments, it could be possible to postulate a schematic reaction mechanism for the SCR of NO over the four Cu–Fe-PILC catalysts studied, as all samples showed similar adsorption bands. However, depending on the Cu species present and their distribution, different steps would be favoured. Thus, in samples where isolated Cu^{2+} ions are

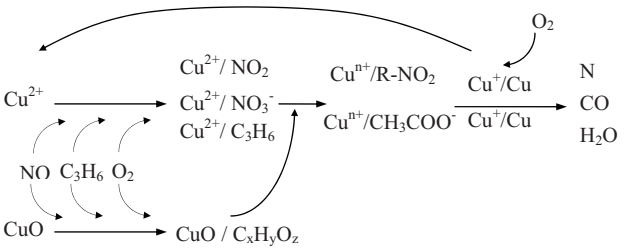

Fig. 8. Possible reaction mechanism scheme for the C_3H_6–SCR of NO over Cu–Fe-PILC catalysts.

homogeneously dispersed, it would be mainly favoured the formation and adsorption of bidentate nitrates. Catalysts with Cu^{2+} and CuO aggregates in accessible positions would promote the hydrocarbon oxidation at low temperature, leading to the formation of $C_xH_yO_zN$ compounds, as well as the monodentate nitrates and nitrites and nitro groups adsorption. The possible reaction mechanism scheme is represented in Fig. 8. The first step of this mechanism would be the NO oxidation to NO_2 species or nitrates with higher oxidation strength. Nitrates species could be anchored as monodentate or bidentate depending on the position of the metal sites, since the Cu^{2+} ions can be isolated or near to CuO clusters. The hydrocarbon adsorption would be considered as the second step. C_3H_6 adsorption is higher on samples with Cu^{2+} and CuO aggregates. Moreover, CuO promotes the hydrocarbon oxidation giving $C_xH_yO_z$ species as reaction intermediates. The next step would be the oxidation of $C_xH_yO_z$ species by the nitro groups and nitrates leading to acetates or $C_xH_yO_zN$ compounds ($R–NO_2$). These last compounds would yield N_2, CO_2 and H_2O, likely via isocyanate, whose fast hydrolysis would give the final products. Copper oxides play an important role in this mechanism since the catalytic activity, at low temperature, was improved by their presence and accessibility.

4. Conclusions

Taking into account the results discussed above the following conclusions can be drawn:

- NO adsorption spectra presented bands attributed to nitrites, nitrates and nitro group. The intensity of those bands was higher when oxygen was present. Bidentate nitrates species were adsorbed on isolated Cu^{2+}, whereas nitro groups, monodentate nitrites and monodentate nitrates were adsorbed on Cu^{2+} ions in positions near to CuO clusters.
- After the exposure of the samples to propene flow, in the absence or in the presence of oxygen, bands assigned to oxidized hydrocarbons appeared. The intensity of these bands was higher in samples with CuO clusters in their structure.
- A general reaction mechanism scheme for the C_3H_6–SCR over Cu–Fe-PILC was postulated. The first step was the NO oxidation to NO_2 or nitrates. The second step was the propene adsorption on active sites. Later, the propene oxidation, which was promoted by CuO aggregates, gave $C_xH_yO_z$. Then, these oxidized hydrocarbons reacted with the nitro species and nitrates leading to acetates or $C_xH_yO_zN$ compounds. Finally, the transformation of the later yielded N_2, CO_2 and H_2O as final products.

Acknowledgments

Financial support from the Ministerio de Ciencia y Tecnología of Spain (Project CTQ-2004-07350-C02-O) and the Consejería de Ciencia y Tecnología de la Junta de Comunidades de Castilla-La Mancha (Proyect PBI-05-038) are gratefully acknowledged.

References

[1] N.W. Cant, I.O.Y. Liu, Catal. Today 63 (2000) 133–146.
[2] C. Yokoyama, M. Misono, J. Catal. 150 (1994) 9–17.
[3] T. Beutel, B. Adelman, W.H.M. Sachtler, Catal. Lett. 37 (1996) 125–130.
[4] R. Burch, P.J. Millington, Appl. Catal. B. 2 (1993) 101–116.
[5] B.K. Cho, J. Catal. 155 (1995) 184–195.
[6] F. Poignant, J.L. Freysz, M. Durati, J. Saussey, Catal. Today 70 (2001) 197–211.
[7] L. Capek, K. Novoveska, Z. Sobalik, B. Wichterlová, L. Cider, E. Jobson, Appl. Catal. B 60 (2005) 201–210.
[8] L. Li, F. Zhang, N. Guan, M. Richter, R. Fricke, Catal. Commun. 8 (2007) 583–588.
[9] K.-I. Shimizu, H. Kawabata, H. Maeshima, A. Satsuma, T. Hattori, J. Phys. Chem. B 104 (2000) 2885–2893.
[10] Y. Chi, S.S.C. Chuang, J. Catal. 190 (2000) 75–91.
[11] M. Sirilumpen, R.T. Yang, N. Tharapiwattananon, J. Mol. Catal. A 137 (1999) 273–286.
[12] J.L. Valverde, A. de Lucas, F. Dorado, A. Romero, P.B. García, J. Mol. Catal. A 230 (2005) 23–28.
[13] F. Dorado, A. de Lucas, P.B. García, J.L. Valverde, A. Romero, Appl. Catal. B 65 (2006) 175–184.
[14] J.L. Valverde, A. Romero, R. Romero, P.B. García, M.L. Sánchez, I. Asencio, Clays Clay Miner. 53 (6) (2005) 613–621.
[15] F. Dorado, A. de Lucas, P.B. García, A. Romero, J.L. Valverde, App. Catal. A 305 (2006) 189–196.
[16] J.L. Valverde, P. Sánchez, F. Dorado, C.B. Molina, A. Romero, Micropor. Mesopor. Mater. 54 (2002) 155–165.
[17] L.S. Cheng, R.T. Yang, Adsorption 1 (1995) 61–75.
[18] K. Hadjiivanov, Catal. Rev. Sci. Eng. 42 (2000) 71–144.
[19] A.A. Davydov, Infrared Spectroscopy of Adsorbed Species on the Surface of Transition Metal Oxides, John Wiley & Sons, New York, 1990.
[20] B.I. Mosqueda Jiménez, A. Jentys, K. Sesham, J.A. Lercher, Appl. Catal. B 46 (2003) 189–202.
[21] G. Mul, A. Zwijnenburg, B. van der Linden, M. Makkee, J.A. Moulijn, J. Catal. 201 (2001) 128–137.
[22] A. Satsuma, K.-I. Shimizu, Prog. Energy Combust. Sci 29 (2003) 71–84.
[23] D.K. Captain, M.D. Amiridis, J. Catal. 194 (2000) 222–232.
[24] W. Shieβer, H. Vinek, A. Jentys, Appl. Catal. B 33 (2001) 263–274.
[25] Z. Schay, V.M. James, G. Pál-Borbély, A. Beck, A.V. Ramaswamy, L. Guczi, J. Mol. Catal. A 162 (2000) 191–198.
[26] G. Delahay, A. Guzmán-Vargas, B. Coq, Appl. Catal. B 70 (2007) 45–52.
[27] M. Huuhtanen, T. Kolli, T. Maunula, R.L. Keiski, Catal. Today 75 (2002) 379–384.
[28] K. Hadjiivanov, B. Boyko Tsyntsarski, T. Nikolova, Phys. Chem. Chem. Phys. 1 (1999) 4521–4528.
[29] F. Dorado, A. de Lucas, P.B. García, A. Romero, J.L. Valverde, I. Asencio, Ind. Eng. Chem. Res. 44 (2005) 8988–8996.